Journal of Materials Chemistry A

Impact of Fluorination Degree of Ether-Based Electrolyte Solvent on Li-metal Battery Performance

Journal:	*Journal of Materials Chemistry A*
Manuscript ID	TA-ART-09-2023-005535.R1
Article Type:	Paper
Date Submitted by the Author:	16-Nov-2023
Complete List of Authors:	Lin, Yangju; Stanford University, Chemical Engineering Yu, Zhiao; Stanford University, Yu, Weilai; Stanford University, Chemical Engineering Liao, Sheng-Lun; Stanford University, Chemical Engineering Zhang, Elizabeth; Stanford University, Materials Science and Engineering Guo, Xuelin; Stanford University, Chemical Engineering Huang, Zhuojun; Stanford University, Materials Science and Engineering Chen, Yuelang; Stanford University, Chemistry Qin, Jian; Stanford University, Chemical Engineering Cui, Yi; Stanford University, Materials Science and Engineering Bao, Zhenan; Stanford University, Chemical Engineering

ARTICLE

Impact of Fluorination Degree of Ether-Based Electrolyte Solvent on Li-metal Battery Performance

Received 00th January 20xx,
Accepted 00th January 20xx

DOI: 10.1039/x0xx00000x

Yangju Lin,[a‡] Zhiao Yu,[a,b‡] Weilai Yu,[a] Sheng-Lun Liao,[a] Elizabeth Zhang,[a,c] Xuelin Guo,[a] Zhuojun Huang,[a,c] Yuelang Chen,[a,b] Jian Qin,*[a] Yi Cui*[c,d,e] and Zhenan Bao*[a]

Electrolytes using fluorinated solvents have proven effective in improving the cycling life of Li-metal batteries, by forming a robust solid-electrolyte interphase through decomposition of anion and fluorinated solvent molecules. Herein, we modulated the fluorination degree of ether-based electrolyte solvents to investigate their performance in Li-metal batteries. We tuned the fluorination degree by installing a monofluorine substituent on one ethoxy group of 1,2-diethoxyethane (DEE) and varying the fluorination degree on the other one, providing three fluorinated DEE solvent molecules (i.e., **F1F0**, **F1F1** and **F1F2**) with a relatively low fluorination degree. All the three electrolytes showed improved solvation strength and ionic conductivities compared with previous highly fluorinated DEE electrolytes, while retaining good oxidative stability. Full cell test using Li-metal anode and nickel-rich cathode revealed that a higher degree of fluorination is beneficial to the cycling performance, and the cycling stability follows **F1F0** < **F1F1** < **F1F2**. Specifically, **F1F0** exhibited poor cycling stability due to its instability against both anode and cathode. While **F1F1** and **F1F2** both showed good stability against Li-metal anode, their relative long-term oxidative stability was responsive for the distinct performance, in which the cycle numbers at 80% capacity retention for **F1F1** and **F1F2** were ~20 and ~80, respectively. Finally, we demonstrated that **F1F2** was able to achieve 90 cycles before reaching 80% capacity retention in practice lithium iron phosphate (LFP) pouch cells. This work shows the importance to modulate the fluorination degree of electrolyte solvents, and this approach is suitable for various cathode materials.

Introduction

The high number of transferring electron per atomic mass and low electrochemical potential in Li^+/Li redox reaction render Li metal an ideal anode material for high-energy-density batteries.[1-3] Despite these merits, the Li-electrolyte side reactions, inaccessible lithium (or called dead lithium) generated during the plating/stripping cycles[4, 5] and, thus, the poor Coulombic efficiency (CE) and cyclability have significantly impeded the practical implementation.[6] A key factor enabling stable Li deposition is the formation of a robust solid electrolyte interphase (SEI) that allows for efficient Li^+ transfer and uniform Li deposition.[7, 8] Typically, this SEI layer is composed of species associated with electrochemical and chemical decomposition of salt and solvent molecules, and a SEI layer that is rich in inorganic components (e.g., LiF, Li_2O and Li_3N) has been found beneficial.[9]

A variety of molecular engineering strategies for electrolytes have been explored in order to achieve robust SEI layers in Li-metal batteries,[10, 11] including additive-reinforced electrolytes (AREs),[12] high concentration electrolytes (HCEs),[13] localized high concentration electrolytes (LHCEs),[14] weakly solvating electrolytes (WSEs),[15-22] and electrolytes with fluorinated solvents,[23-29] etc. In these approaches, the formation of a robust SEI layer is promoted through decomposition of either additive, anion or/and fluorinated molecules. In particular, the fluorinated solvents were found to simultaneously provide several merits in electrolytes, including 1) improved oxidative stability resulted from the high electron-withdrawing capability of fluorine that lowers the highest occupied molecular orbital (HOMO),[30, 31] 2) promotion of anion-derived SEI layer due to the weakened solvation ability associated with the reduced electron density of binding atoms,[32] 3) improved flame retardance,[33] and 4) enriched LiF component in SEI layer through potential decomposition of solvent molecules.[34, 35] Notably, the strategy of solvent fluorination allows for a single-solvent low-concentration electrolyte system without compromising ionic conductivity.[36-38]

Examples of using fluorinated molecule as a single electrolyte solvent include a series of long-chain fluorinated glymes,[39, 40] fluorinated 1,4-dimethoxylbutane (FDMB),[41] *N*, *N*-dimethylsulfamoyl fluoride (FSA),[34] *N*, *N*-dimethyltrifluoromethane-sulfonamide (DMTMSA),[31] fluorinated-1,2-diethoxyethane (FDEE)[32] and, more recently, 1,1,1-trifluoro-2,3-dimethoxypropane (TFDMP)[42] and bis(2-fluoroethyl) ethers (BFE).[43] In addition to improved oxidative

[a] *Department of Chemical Engineering,* [b] *Department of Chemistry,* [c] *Department of Materials Science and Engineering,* [d] *Department of Energy Science and Engineering, Stanford University, Stanford, California 94305, United States.*
[e] *Stanford Institute for Materials and Energy Sciences, SLAC National Accelerator Laboratory, Menlo Park, California 94025, United States.*
E-mail: *zbao@stanford.edu; yicui@stanford.edu; jianq@stanford.edu*
Electronic Supplementary Information (ESI) available: [details of any supplementary information available should be included here]. See DOI: 10.1039/x0xx00000x

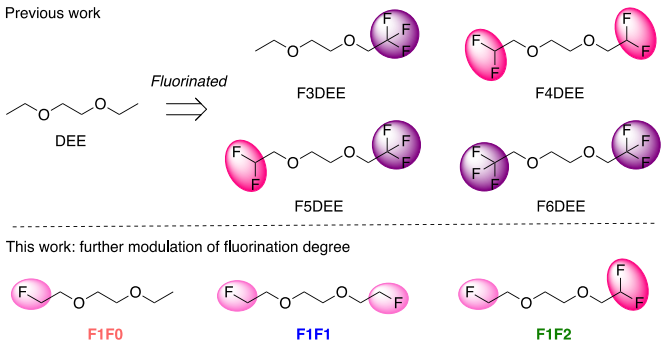

Figure 1 Chemical structures of fluorinated 1,2-diethoxyethane solvent molecules.

stability, all these electrolytes showed excellent CE and cyclability using nickel-rich high-voltage cathodes. We recently showed that an exciting family of electrolyte based on FDEE (Figure 1 top row) can achieve Li-cycling CE as high as 99.9% and ~200 cycles of full battery cycling at high-loading capacity (4.8 mAh/cm^2) under hash cycling conditions (0.2C charge, 0.3C discharge).[32] This series electrolytes have fluorine content of 3-6 fluorine atoms per molecule and show moderate ionic conductivities, and a higher ionic conductivity is necessary for fast charging/discharging. Therefore, we sought to fine-tune the degree of fluorination of DEE in the lower fluorine regime (Figure 1 bottom row) to optimize the ionic conductivity with the hope to not compromise their oxidative stability.

It is known that increased fluorination degree in ether molecule improves oxidative stability but simultaneously reduces the solvation/binding strength, resulting in formation of larger size of salt-anion clusters and so reduced ionic conductivity.[32] We therefore further reduced the fluorination degree on the ether molecules, by applying the monofluoro-substitution on the one ethoxy group of 1,2-diethoxyethane (DEE) and varying the number of fluorine substituent on the other one (Figure 1 bottom row).

Results and discussion

Synthesis and characterization of electrolytes

The fluorinated ether molecules (i.e., **F1F0**, **F1F1**, and **F1F2**) are synthesized through S_{N2} reactions and can be obtained in > 10 g scale (see Supporting Information). Three single-solvent electrolytes were prepared by adding 1.2 mmol of lithium bis(fluoromethanesulfonyl)imide (LiFSI) into 1 mL of each of the solvent molecules. We then performed ^{7}Li NMR to analyze the solvation structure of salt in the electrolyte using LiCl in D_2O as an internal reference. As can be seen in Figure 2a, the chemical shift of ^{7}Li gradually moved up field upon increasing the degree of fluorination. This increased electron shielding is attributed to more compact cation-anion interaction resulted from weakened solvation ability, as has been observed in other fluorinated solvents, HCEs, LHCEs and WSEs.[16, 32, 43] Herein, consistent with our expectation, increasing the fluorination degree of ether solvent reduces its solvation ability; however, the impact on chemical shifts are not as pronounced as those of highly fluorinated FDEE electrolytes (Figure 1, top),[32] indicating

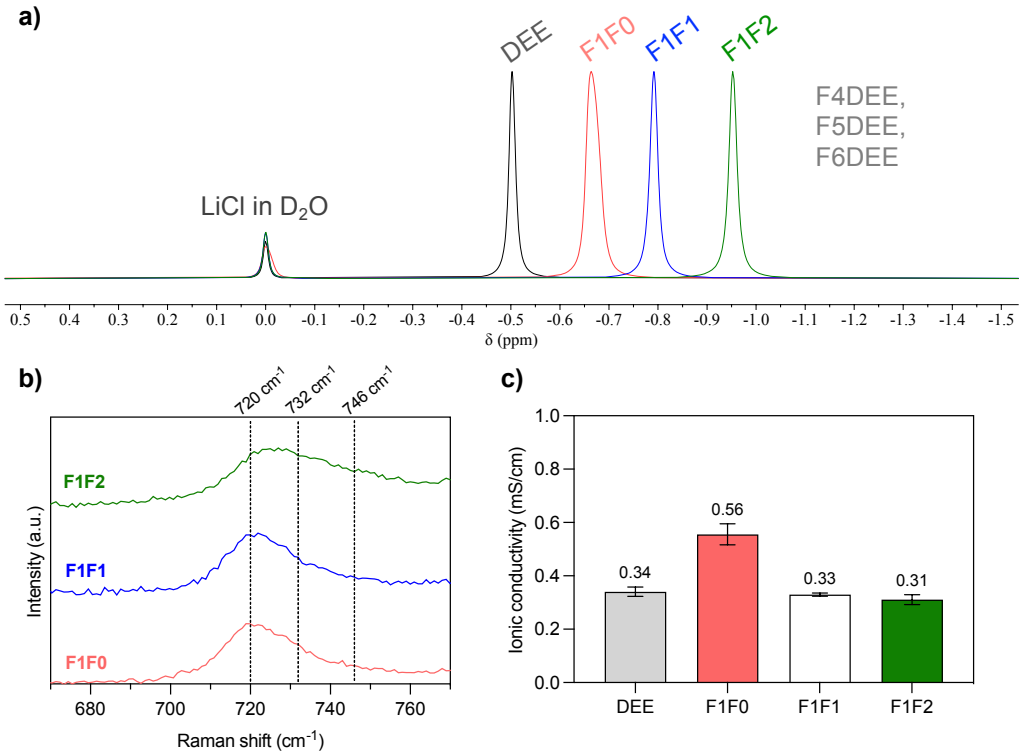

Figure 2 a) Overlay of normalized ^{7}Li NMR spectra of electrolyte solutions containing 1.2 mole/L of LiFSI salt, and LiCl in D_2O was applied as an internal standard. The pale blue region indicates the chemical shift of F4DEE, F5DEE and F6DEE electrolytes in previous report. b) Raman spectra of electrolytes in this study showing the solvation conditions of LiFSI salt. c) Comparison of ionic conductivity in the stainless steel-separator-stainless steel sandwich structure using Celgard2325 trilayer separator. Each electrolyte was measured three times (see Table S3).

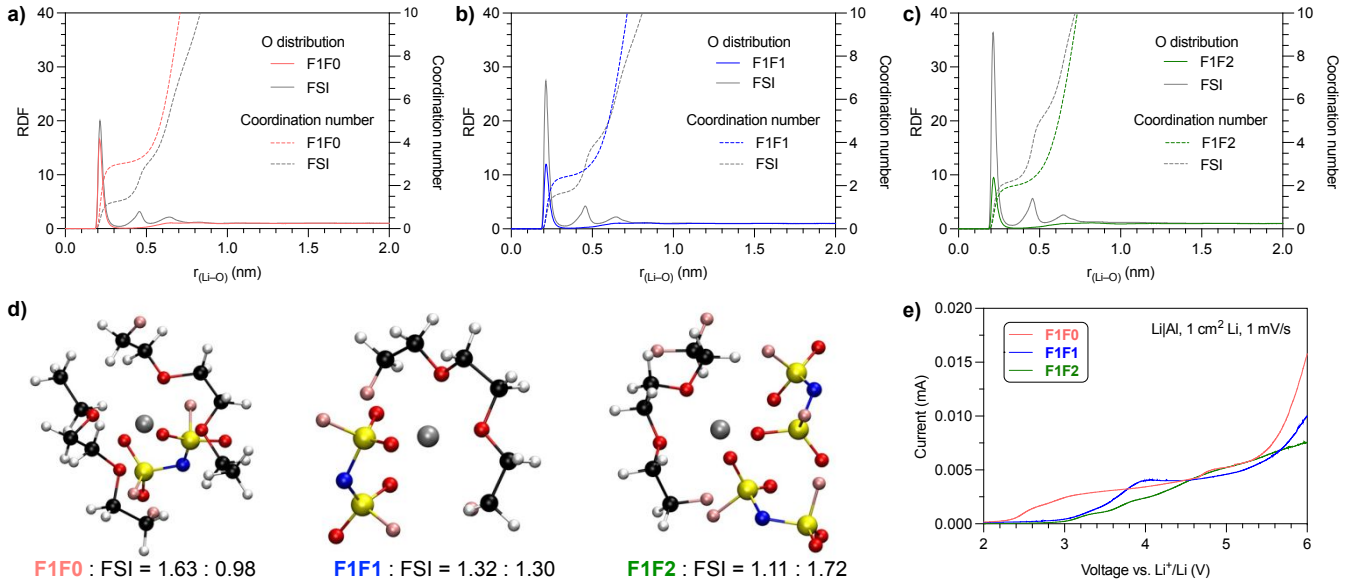

Figure 3 Radial distribution function of O atoms of a) **F1F0**, b) **F1F1** and c) **F1F2** solvent and anion over the distance from Li^+ cation center. d) Representative solvation structure of electrolytes with 1.2 mol/L LiFSI salt, and the average numbers of solvent and anion in the solvation structure are indicated at the bottom. e) Oxidative stability of electrolytes against Al current collector (scanning rate: 1 mV/s).

improved salt solvation (or cation-anion dissociation) in our new electrolytes. Additional evidence from Raman measurement (Figure 2b) showed that **F1F0** and **F1F1** electrolytes exhibit mainly solvent separated ion pairs (SSIPs, 720 cm^{-1}),while trivial contact ion pairs (CIPs, 732 cm^{-1}) and aggregates (AGGs, 746 cm^{-1}).[44] In the case of **F1F2**, the broad shoulder peak indicated significant portion of CIPs and AGGs, suggesting the weakened solvation strength.

To evaluate the ionic conductivity, we inflated the electrolyte solution into a Celgard2325 separator and used stainless-steel-sandwich configuration to memetic the conditions of coin-cell tests. As shown in Figure 2c, all three electrolytes exhibited relatively higher ionic conductivities compared with previous FDEE counterparts (0.05–0.17 mS/cm),[32] and they follow the trend **F1F0** > **F1F1** > **F1F2**, in alignment with the solvation strength. Interestingly, **F1F0** showed ionic conductivity that is even higher than the nonfluorinated DEE electrolyte. We reasoned that the F substituent increases the polarity of molecule and provides an additional binding to the Li^+, giving rise to less compact cation-anion cluster, as indicated by ^{19}F NMR spectra (Figure S1) and some previous studies.[43, 45] Macroscopically, the molecular solvation is reflected in the electrolyte viscosities, where the viscosity trend follows: **F1F0** < **F1F1** < **F1F2** (Table S2), and a relative higher viscosity leads to a lower diffusivity and so lower ionic conductivity.

Computation of solvation structures

We further performed molecular dynamics (MD) simulation to gain insight into the solvation behavior. Figure 3a-c showed the probability of coordinating O atom as a function of distance from the Li^+ center, or radial distribution function (RDF). We compared the O atom from both solvent and anion molecules. The first solvation shell peaked at $r_{(Li-O)}$ ~ 0.22 nm, which indicates the length of Li–O dative bond,[46] for both solvent and anion in all three electrolyte systems.

Notably, the composition of solvating O atom from solvent and anion molecules varied with the fluorination degree of electrolyte solvent. The fraction of solvating O atom from FSI anion increases in the order **F1F0** < **F1F1** < **F1F2**, and that from solvent molecule decreases accordingly. This trend is consistent with the ordering of the solvation strength. Consequently, the overall cation-anion interaction is stronger in less solvated electrolyte system, as also evidenced by ^7Li NMR and Raman spectra analysis (Figure 2a and 2b).

To present a quantitative picture of solvation shell, we integrated the RDF to get the coordinating number (CN) of O atoms from solvent and FSI anion. The presence of a plateau at $r_{(Li-O)}$ ~ 0.36 nm for both solvent and FSI anion suggested the radius of first solvation sheath, and the corresponding CN in the sheath was estimated. For **F1F0** electrolyte, the CNs of O from solvent and FSI anion are 3.03 and 1.34, respectively. The numbers became 2.46 and 1.76 for **F1F1** electrolyte, and 2.03 and 2.31 for **F1F2** electrolyte. We further counted the number of solvent and FSI anion molecules in the first solvation shell and found, on average, 1.63 solvent and 0.98 FSI in **F1F0** electrolyte, 1.32 solvent and 1.30 FSI in **F1F1** electrolyte, and 1.11 solvent and 1.72 FSI in **F1F2** electrolyte. It is worth noting that for electrolytes with 1.2 mmol of LiFSI in 1 mL solvent, the solvent/LiFSI molar ratios are 6.01, 6.03 and 5.78 for **F1F0**, **F1F1** and **F1F2**, respectively. Hence, there are both "binding" and "free" solvent molecules in the electrolytes. The above quantitative analysis is further highlighted by the typical solvation structures shown in Figure 3d. Again, this observation is in alignment with the relative solvation strength of solvent molecules.

Previous work have found strong correlation between solvation structure and the oxidative stability of electrolytes.[13-29] We then scrutinized the impact of fluorination degree of

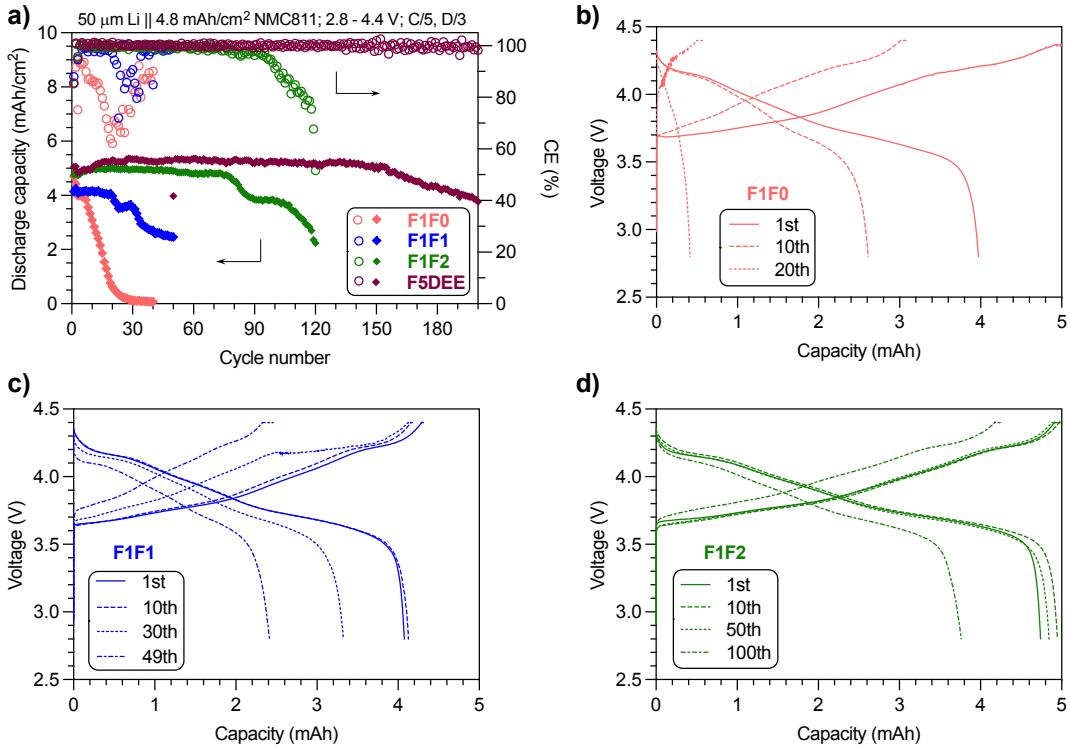

Figure 4 a) Capacity and CE retention of **F1F0**, **F1F1** and **F1F2** electrolytes over cycling number. The data of F5DEE was adapted from previous results.[32] The charge/discharge curves of b) **F1F0**, c) **F1F1** and d) **F1F2** at various cycles. Note: cycling of full cells were repeated and results can be found in Figure S4-7.

solvent on the oxidative stability and, hence, the feasibility to be used in high-voltage battery systems. Figure 3e shows the screening of leakage current through linear sweep voltammetry of Li||Al half cells at the scanning rate of 1 mV/s. Interestingly, all three electrolytes exhibit a relatively small current (< 5 μA) at up to 5 V, and these observed low leakage current are comparable to previous FDEE electrolytes.[32]

Li-metal full battery performance

Encouraged by the improved ionic conductivity and retained anodic stability while reducing the fluorination degree, we performed Li||NMC811 full battery tests of the three electrolytes using the same conditions as reported for FDEE electrolytes, i.e., pairing 50-μm-thick Li foil (10.3 mAh/cm^2) with high-loading NMC811 cathode (4.8 mAh/cm^2) to yield a negative-to-positive electrode ratio (N/P) of ~2.1; using electrolyte-to-cathode ratio (E/C) of ~8 g/Ah; and cycling at C/5 charging and C/3 discharging rates, for the purpose of comparison with previous studies and so evaluation of fluorination effects.

A representative set of battery cycling results is provided in Figure 4a (repeated results are provided in Figure S4-7), and a clear trend of cycling life was observed: **F1F0** < **F1F1** < **F1F2**. The capacity of **F1F0** decayed quickly to near zero within 30 cycles, and its CE dropped significantly despite the presence of excess Li reservoir, indicating the instability of **F1F0** against both anode and cathode. Additionally, the decay pattern is in contrast to the DEE electrolyte (non-fluorinated electrolyte), which presents a steady capacity without significant reduction in the beginning 18 cycles and then drop quickly to 80% capacity in the following 37 cycles.[16] Herein, the continuous capacity decay in **F1F0** suggested the negative impact of mono-fluorination on DEE. As for **F1F1**, the capacity remained almost unchanged in the first 20 cycles but then quickly reduced over cycles. In stark contrast, **F1F2** exhibited stable cycling without substantial capacity decay for ~80 cycles, which is comparable to F3DEE and F6DEE but less than F4DEE and F5DEE in previous report.[32]

We further studied the charge/discharge curves at different cycles. Figure 4b shows the charge/discharge curves of **F1F0** at 1st, 10th and 20th cycles, where the overpotential at the start of charge/discharge remains nearly unchanged while the capacity fades quickly over cycles, indicating the retained bulk and interfacial resistance yet instability against electrodes. Specifically, the 10th discharge process only gave ~2.6 mAh, which corresponds to ~84% of the 10th charging capacity (~3.1 mAh). Because the high initial Li reservoir (N/P ~ 2.1) would guarantee the 3.1 mAh capacity when discharge at the 10th cycle, the observed capacity loss highly suggested the cathode degradation during the 10th discharge cycle. Indeed, the XRD analysis of cathode after 10 cycles using **F1F0** electrolyte indicated significant layer disruption (Figure S8). This instability can be ascribed to the intrinsic low oxidative stability of **F1F0** (as will be discussed later), and the resulting side reactions deteriorates the cathode integrity. In contrast, **F1F1** showed slightly less capacity loss over cycles, but a substantial polarization (decrease in the initial discharge voltage or increase in charge voltage) imply the raised bulk and interfacial resistance. In the case of **F1F2**, the capacity loss is even less and the polarization over cycles is not as pronounced. Therefore,

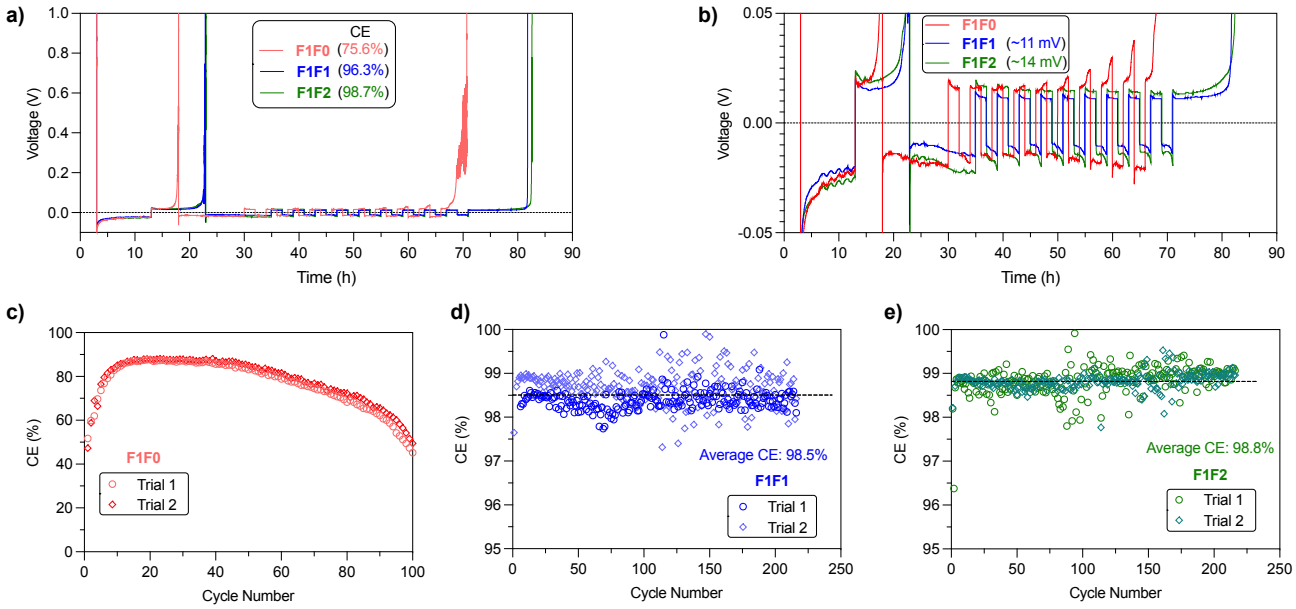

Figure 5 a) CE evaluation of Li||Cu half cells using modified Aurbach method. b) Zoom-in view of voltage-time profiles in CE measurements. CE values of c) **F1F0**, d) **F1F1** and e) **F1F2** electrolytes over long-term cycling of Li||Cu half cells. The average CE of **F1F1** and **F1F2** from two trials over > 200 cycles are indicated in d) and e), respectively.

compared with **F1F0**, the improved oxidative stability of **F1F1** benefited the cathode performance but induced polarization, and **F1F2** overcame both drawbacks. We postulated that the combined compact Li^+-anion pairs associated with weak solvation and improved oxidative stability resulted from increased fluorination degree contributed to the overall improved cycling performance. Although the ionic conductivity of **F1F1** and **F1F2** are similar, the polarization evolved distinctly and could be attributed to several factors, including the quality of generated interphase layer at both anode (SEI) and cathode (CEI) and their dissolution conditions, changes in electrolyte contents due to the interphase dissolution and the generated byproducts associated with electrochemical/chemical decomposition of solvent and/or salt.

Analysis of Li-metal half-cell cycling

We then examined the stability of Li metal cycling through Li||Cu half cells. Typical evaluation of CE using the modified Aurbach method[47] indicated that the CEs for **F1F0**, **F1F1**, and **F1F2** are 75.8%, 96.3% and 98.7%, respectively (Figure 5a). A close scrutinization of the overpotential curves reveals a "yielding" peak in the stripping cycle for all three electrolytes (Figure 5b), which is ascribed to the transformation of interphase kinetics.[48] Meanwhile, we noticed a significant capacity loss in the beginning cleaning cycle of **F1F0**, along with slowly increased stripping overpotential in the later cycles, indicating cathodic instability of **F1F0** and impedance increase. Notably, the overpotential curve of stripping cycle presents spike features, which could be related to the reconnection of "dead" Li upon stripping.[49] We therefore reasoned that **F1F0** presents poor electrochemical stability and unstable/nonuniform Li deposition. By contrast, **F1F1** and **F1F2** showed relatively high CE of 96.3% and 98.7%, respectively, and the average overpotential of **F1F1** and **F1F2** under 0.5 mA/cm^2 current are respectively 11 mV and 13 mV, both of which are lower than F5DEE (~20 mV)[32] owing to their higher ionic conductivity.

Long-term cycling of Li||Cu half cells was applied to further validate the Li cycling stability (Figure 5c-e). Interestingly, **F1F0** showed extremely low CE of ~50% in the first cycle, and it then increased and reached a plateau value of ~88% in the following 20 cycles. However, this value slowly decreased to ~50% after 100 cycles. It was found that the average CE of initial 12 cycles is ~75%, which is consistent with the CE value obtained from the

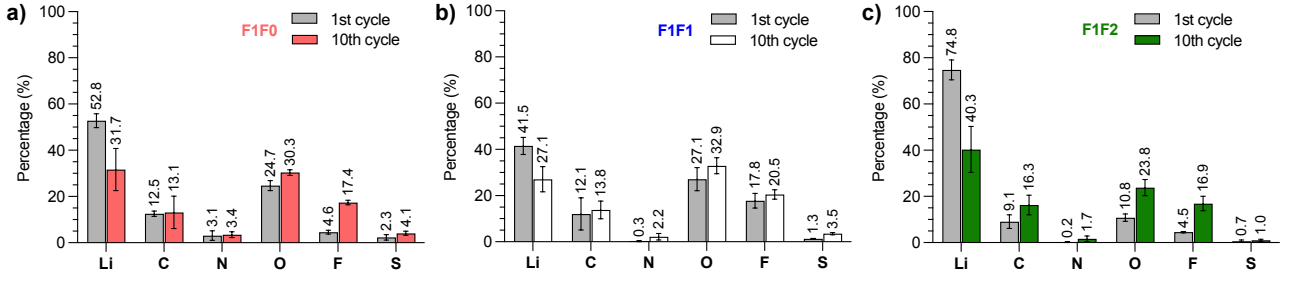

Figure 6 XPS analysis of SEI composition of a) **F1F0**, b) **F1F1**, and c) **F1F2** electrolytes at the 1st and 10th cycles of lithium deposition using Li||Cu half cells. The results were obtained by averaging the signals from 4 different sputtering times.

modified Aurbach measurement that includes 12 cycles of Li plating/stripping. Herein, **F1F0** shows poor stability against Li cycling and thus cycling of full battery. On the other hand, both **F1F1** and **F1F2** showed stable Li cycling over 200 cycles and average CE of 98.5% and 98.8%, respectively. It is worth noticing that the CE of both **F1F1** and **F1F2** quickly reached to stable values during the initial 3 cycles, which suggests a quick passivation and formation of robust SEI layers (Figure S9).

Despite the similar Li||Cu cycling performance between **F1F1** and **F1F2**, they show different full battery performance. To understand the underlying mechanism, we compared the Li deposition morphology of **F1F1** and **F1F2**. However, no substantial difference in the grain size and morphology was found (Figure S10). Further, the SEI composition after one cycle was analyzed by X-ray photoelectron spectroscopy (XPS), which showed signals from LiOH, Li_2O, LiF, Li_2SO_x, Li_2S and organic species for both electrolytes (Figure S11-13). While the species are similar, a closer comparison of relative abundance of each element revealed that the O and F contents in **F1F1** is relatively higher than **F1F2** after the first cycle (27.1% vs. 10.8% and 17.8% vs. 4.5%, Figure 6). The difference could be due to the higher electrochemical susceptibility of monofluoride substituent than difluoro one. It is worth noticing that the observed SEI content by XPS is an evaluation of results from multiple factors: 1) the electrolyte solvation dictates the generated SEI composition; 2) the dissolution of SEI in the corresponding electrolyte. Direct comparison of SEI contents between different electrolytes seems less meaningful in elucidating their relative performance, as the observed contents are the "stable" residue in the specific electrolyte.

We next scrutinized the SEI composition for each individual electrolyte at the 10th cycle. It was found that the O and F contents in **F1F1** slightly increased to 32.9% and 20.5%, respectively. Therefore, the potential stable inorganic species of **F1F1** maintained at high content over cycles. Interestingly, the raise was more significant in **F1F2**, which showed 23.8% for O and 16.9% for F at the 10th cycle. The increase of O and F contents in **F1F2** over cycling indicated more accumulation of stable components (possibly Li_2O and LiF) in the SEI, which we hypothesized could be a consequence of less SEI dissolution over cycling,[50] and the dissolved SEI components could potentially migrate to the cathode side and affect the cathode performance.[51]

Long-term oxidative stability

The SEI composition and Li||Cu half-cell cycling performance of **F1F1** and **F1F2** are rather similar, and albeit thin, the Li metal foil in the full cell still provides excess Li reservoir. Therefore, with an average CE of > 98% for Li plating/stripping, the full cell performance is more limited by the cathode side. Because full cell cycling is a long-term process, the oxidation of electrolytes occurs in an accumulating manner and the side reactions could diminish the cathode integrity over time. We therefore performed chronoamperometry to understand the long-term oxidative stability of electrolytes under high voltage. Figure 7 shows the leakage current of electrolytes under 4.4 V constant voltage over time using Li||Pt half cells. Significant leakage current was observed in **F1F0** and **F1F1** over long-term high voltage holding, and the situation devastated over time. By contrast, there was minimal leakage current in **F1F2**, and it remained steady over more than 18 h. Herein, compared with **F1F1**, the superior oxidative stability of **F1F2** is responsible for its much more stable cycling of full batteries.

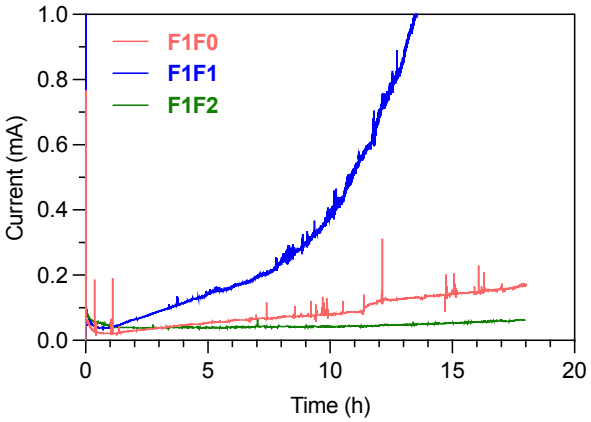

Figure 7 The leakage current of electrolytes under 4.4V constant voltage holding.

Performance of anode-less pouch cells

To evaluate the application of these new electrolytes in practical cells, we performed cycling test of commercial multilayer anode-less LFP pouch cell with relative high area loading of 2.1 mAh/cm^2. As shown in Figure 8, the ~80% capacity retention using **F1F1** electrolyte was achieved at ~55 cycles. With improved oxidative stability, **F1F2** was able to realize ~90 cycles. For comparison, the state-of-the-art electrolyte F5DEE achieved a high cycle number of ~110. Therefore, albeit it can not outperform the F5DEE electrolyte, the **F1F2** electrolyte is suitable for research in practice cells.

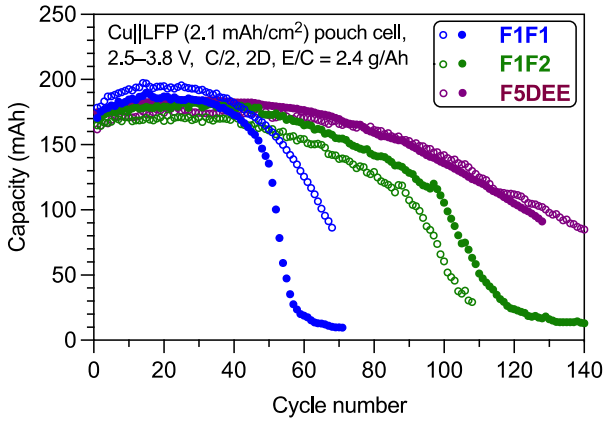

Figure 8 Long-term cycling of anode-less Cu||LFP pouch cells using **F1F1**, **F1F2** and F5DEE electrolytes. The cycling was performance at 0.5C charging rate and 2C discharging rate.

Conclusions

To conclude, the modulation of fluorination degree in ether-based electrolyte solvents allows for fine-tuning of solvation strength and long-term oxidative stability. A general trend that low degree of fluorination presents relatively strong solvation but poor oxidative stability and increasing fluorination degree improves the oxidative stability at the expense of solvation strength has been observed. Among these ether solvents with relatively low fluorination degree, **F1F0** exhibited particularly poor stability against both Li-metal anode and NMC cathode. While **F1F1** and **F1F2** showed comparable cathodic stability, **F1F2** possessed better anodic stability and, therefore, enhanced battery cyclability. While the performance of this series of electrolytes does not outperform our previous FDEE electrolytes, the improved ionic conductivity might be beneficial to high-current density (> 1 mAh/cm^2, Figure S9) charging of battery systems that possess relatively low overpotential.

The observed trade-off between ionic conductivity (or related solvation capability) and oxidative stability makes it challenging to design an ideal single solvent through solely tuning of fluorination degree. Strategies that can further enhance the electrolyte performance include increasing salt concentration, where there would be a point that provides optimal conductivity and improved oxidative stability, and adding diluent, as has been demonstrated recently by Ren and coworkers for the **F1F1** solvent molecule.[45]

Author Contributions

Yangju Lin and Zhiao Yu contributed equally to this work. Yangju Lin: conceptualization, methodology, investigation, data curation, visualization, writing – original draft; Zhiao Yu: conceptualization, investigation, methodology, data curation; Weilai Yu: investigation, data curation, visualization; Sheng-Lun Liao: methodology, formal analysis; Elizabeth Zhang, Xuelin Guo, Zhuojun Huang, and Yuelang Chen: data curation; Jian Qin: supervision, discussion, writing - review and editing; Yi Cui: supervision, discussion, writing - review and editing; Zhenan Bao: supervision, project administration, discussion, writing - review and editing. The manuscript was reviewed and edited by all the above authors. All authors have given approval to the final version of the manuscript.

Conflicts of interest

Zhenan Bao, Yi Cui, Yangju Lin, Zhiao Yu and Yuelang Chen declare that this work is part of US Provisional Patent Application filed in 2021. The remaining authors declare no competing interests.

Acknowledgements

This work was supported by the Assistant Secretary for Energy Efficiency and Renewable Energy, Office of Vehicle Technologies of the U.S. Department of Energy, under the Battery 500 Consortium and the Battery Materials Research (BMR) programs.

References

1. Y. Guo, H. Li and T. Zhai, *Adv Mater*, 2017, **29**.
2. D. Lin, Y. Liu and Y. Cui, *Nat Nanotechnol*, 2017, **12**, 194-206.
3. W. Xu, J. Wang, F. Ding, X. Chen, E. Nasybulin, Y. Zhang and J.-G. Zhang, *Energy & Environmental Science*, 2014, **7**, 513-537.
4. C. Fang, J. Li, M. Zhang, Y. Zhang, F. Yang, J. Z. Lee, M. H. Lee, J. Alvarado, M. A. Schroeder, Y. Yang, B. Lu, N. Williams, M. Ceja, L. Yang, M. Cai, J. Gu, K. Xu, X. Wang and Y. S. Meng, *Nature*, 2019, **572**, 511-515.
5. P. P. Paul, E. J. McShane, A. M. Colclasure, N. Balsara, D. E. Brown, C. Cao, B.-R. Chen, P. R. Chinnam, Y. Cui, E. J. Dufek, D. P. Finegan, S. Gillard, W. Huang, Z. M. Konz, R. Kostecki, F. Liu, S. Lubner, R. Prasher, M. B. Preefer, J. Qian, M.-T. F. Rodrigues, M. Schnabel, S.-B. Son, V. Srinivasan, H.-G. Steinrück, T. R. Tanim, M. F. Toney, W. Tong, F. Usseglio-Viretta, J. Wan, M. Yusuf, B. D. McCloskey and J. Nelson Weker, *Advanced Energy Materials*, 2021, **11**, 2100372.
6. X. B. Cheng, R. Zhang, C. Z. Zhao and Q. Zhang, *Chem Rev*, 2017, **117**, 10403-10473.
7. M. D. Tikekar, S. Choudhury, Z. Tu and L. A. Archer, *Nature Energy*, 2016, **1**, 16114.
8. E. Peled and S. Menkin, *Journal of The Electrochemical Society*, 2017, **164**, A1703.
9. X. B. Cheng, R. Zhang, C. Z. Zhao, F. Wei, J. G. Zhang and Q. Zhang, *Adv Sci (Weinh)*, 2016, **3**, 1500213.
10. S. Li, M. Jiang, Y. Xie, H. Xu, J. Jia and J. Li, *Adv Mater*, 2018, **30**, e1706375.
11. Y. Jie, X. Ren, R. Cao, W. Cai and S. Jiao, *Advanced Functional Materials*, 2020, **30**, 1910777.
12. H. Zhang, G. G. Eshetu, X. Judez, C. Li, L. M. Rodriguez-Martínez and M. Armand, *Angewandte Chemie International Edition*, 2018, **57**, 15002-15027.
13. Y. Yamada, J. Wang, S. Ko, E. Watanabe and A. Yamada, *Nature Energy*, 2019, **4**, 269-280.
14. X. Cao, H. Jia, W. Xu and J.-G. Zhang, *Journal of The Electrochemical Society*, 2021, **168**, 010522.
15. J. Zhang, Q. Li, Y. Zeng, Z. Tang, D. Sun, D. Huang, Y. Tang and H. Wang, *ACS Energy Letters*, 2023, **8**, 1752-1761.
16. Y. Chen, Z. Yu, P. Rudnicki, H. Gong, Z. Huang, S. C. Kim, J.-C. Lai, X. Kong, J. Qin, Y. Cui and Z. Bao, *Journal of the American Chemical Society*, 2021, **143**, 18703-18713.
17. E. Park, J. Park, K. Lee, Y. Zhao, T. Zhou, G. Park, M.-G. Jeong, M. Choi, D.-J. Yoo, H.-G. Jung, A. Coskun and J. W. Choi, *ACS Energy Letters*, 2023, **8**, 179-188.
18. H. Zhang, Z. Zeng, F. Ma, Q. Wu, X. Wang, S. Cheng and J. Xie, *Angew Chem Int Ed Engl*, 2023, DOI: 10.1002/anie.202300771, e202300771.
19. T. D. Pham and K.-K. Lee, *Small*, 2021, **17**, 2100133.
20. R. Xu, J.-F. Ding, X.-X. Ma, C. Yan, Y.-X. Yao and J.-Q. Huang, *Advanced Materials*, 2021, **33**, 2105962.
21. K. Ding, C. Xu, Z. Peng, X. Long, J. Shi, Z. Li, Y. Zhang, J. Lai, L. Chen, Y.-P. Cai and Q. Zheng, *ACS Applied Materials & Interfaces*, 2022, **14**, 44470-44478.
22. Z. Li, H. Rao, R. Atwi, B. M. Sivakumar, B. Gwalani, S. Gray, K. S. Han, T. A. Everett, T. A. Ajantiwalay, V. Murugesan, N. N. Rajput and V. G. Pol, *Nature Communications*, 2023, **14**, 868.
23. N. von Aspern, G. V. Röschenthaler, M. Winter and I. Cekic-Laskovic, *Angew Chem Int Ed Engl*, 2019, **58**, 15978-16000.

24. Y. Zhao, T. Zhou, T. Ashirov, M. E. Kazzi, C. Cancellieri, L. P. H. Jeurgens, J. W. Choi and A. Coskun, *Nature Communications*, 2022, **13**, 2575.
25. Y. Zhao, T. Zhou, M. El Kazzi and A. Coskun, *ACS Applied Energy Materials*, 2022, **5**, 7784-7790.
26. J. Holoubek, M. Yu, S. Yu, M. Li, Z. Wu, D. Xia, P. Bhaladhare, M. S. Gonzalez, T. A. Pascal, P. Liu and Z. Chen, *ACS Energy Letters*, 2020, **5**, 1438-1447.
27. Y. Zhao, T. Zhou, L. P. H. Jeurgens, X. Kong, J. W. Choi and A. Coskun, *Chem*, 2023, **9**, 682-697.
28. Y. Yang, D. M. Davies, Y. Yin, O. Borodin, J. Z. Lee, C. Fang, M. Olguin, Y. Zhang, E. S. Sablina, X. Wang, C. S. Rustomji and Y. S. Meng, *Joule*, 2019, **3**, 1986-2000.
29. J. Shi, C. Xu, J. Lai, Z. Li, Y. Zhang, Y. Liu, K. Ding, Y. P. Cai, R. Shang and Q. Zheng, *Angew Chem Int Ed Engl*, 2023, **62**, e202218151.
30. X. Fan, L. Chen, O. Borodin, X. Ji, J. Chen, S. Hou, T. Deng, J. Zheng, C. Yang, S.-C. Liou, K. Amine, K. Xu and C. Wang, *Nature Nanotechnology*, 2018, **13**, 715-722.
31. W. Xue, M. Huang, Y. Li, Y. G. Zhu, R. Gao, X. Xiao, W. Zhang, S. Li, G. Xu, Y. Yu, P. Li, J. Lopez, D. Yu, Y. Dong, W. Fan, Z. Shi, R. Xiong, C.-J. Sun, I. Hwang, W.-K. Lee, Y. Shao-Horn, J. A. Johnson and J. Li, *Nature Energy*, 2021, **6**, 495-505.
32. Z. Yu, P. E. Rudnicki, Z. Zhang, Z. Huang, H. Celik, S. T. Oyakhire, Y. Chen, X. Kong, S. C. Kim, X. Xiao, H. Wang, Y. Zheng, G. A. Kamat, M. S. Kim, S. F. Bent, J. Qin, Y. Cui and Z. Bao, *Nature Energy*, 2022, **7**, 94-106.
33. Z. Zhang, L. Hu, H. Wu, W. Weng, M. Koh, P. C. Redfern, L. A. Curtiss and K. Amine, *Energy & Environmental Science*, 2013, **6**, 1806-1810.
34. W. Xue, Z. Shi, M. Huang, S. Feng, C. Wang, F. Wang, J. Lopez, B. Qiao, G. Xu, W. Zhang, Y. Dong, R. Gao, Y. Shao-Horn, J. A. Johnson and J. Li, *Energy & Environmental Science*, 2020, **13**, 212-220.
35. W. Zhang, T. Yang, X. Liao, Y. Song and Y. Zhao, *Energy Storage Materials*, 2023, **57**, 249-259.
36. X. Chen and Q. Zhang, *Accounts of Chemical Research*, 2020, **53**, 1992-2002.
37. Z. Li, Y. Chen, X. Yun, P. Gao, C. Zheng and P. Xiao, *Advanced Functional Materials*, 2023, **33**, 2300502.
38. Y. Wang, Z. Li, Y. Hou, Z. Hao, Q. Zhang, Y. Ni, Y. Lu, Z. Yan, K. Zhang, Q. Zhao, F. Li and J. Chen, *Chemical Society Reviews*, 2023, **52**, 2713-2763.
39. P. Ma, P. Mirmira and C. V. Amanchukwu, *ACS Central Science*, 2021, **7**, 1232-1244.
40. C. V. Amanchukwu, Z. Yu, X. Kong, J. Qin, Y. Cui and Z. Bao, *Journal of the American Chemical Society*, 2020, **142**, 7393-7403.
41. Z. Yu, H. Wang, X. Kong, W. Huang, Y. Tsao, D. G. Mackanic, K. Wang, X. Wang, W. Huang, S. Choudhury, Y. Zheng, C. V. Amanchukwu, S. T. Hung, Y. Ma, E. G. Lomeli, J. Qin, Y. Cui and Z. Bao, *Nature Energy*, 2020, **5**, 526-533.
42. Y. Zhao, T. Zhou, M. Mensi, J. W. Choi and A. Coskun, *Nature Communications*, 2023, **14**, 299.
43. G. Zhang, J. Chang, L. Wang, J. Li, C. Wang, R. Wang, G. Shi, K. Yu, W. Huang, H. Zheng, T. Wu, Y. Deng and J. Lu, *Nature Communications*, 2023, **14**, 1081.
44. Y. Yamada, M. Yaegashi, T. Abe and A. Yamada, *Chemical Communications*, 2013, **49**, 11194-11196.
45. D. Ruan, L. Tan, S. Chen, J. Fan, Q. Nian, L. Chen, Z. Wang and X. Ren, *JACS Au*, 2023, **3**, 953-963.
46. O. C. Gagné and F. C. Hawthorne, *Acta Crystallogr B Struct Sci Cryst Eng Mater*, 2016, **72**, 602-625.
47. B. D. Adams, J. Zheng, X. Ren, W. Xu and J.-G. Zhang, *Advanced Energy Materials*, 2018, **8**, 1702097.
48. K. N. Wood, E. Kazyak, A. F. Chadwick, K.-H. Chen, J.-G. Zhang, K. Thornton and N. P. Dasgupta, *ACS Central Science*, 2016, **2**, 790-801.
49. K.-H. Chen, K. N. Wood, E. Kazyak, W. S. LePage, A. L. Davis, A. J. Sanchez and N. P. Dasgupta, *Journal of Materials Chemistry A*, 2017, **5**, 11671-11681.
50. P. Sayavong, W. Zhang, S. T. Oyakhire, D. T. Boyle, Y. Chen, S. C. Kim, R. A. Vilá, S. E. Holmes, M. S. Kim, S. F. Bent, Z. Bao and Y. Cui, *Journal of the American Chemical Society*, 2023, **145**, 12342-12350.
51. H. Wu, H. Jia, C. Wang, J.-G. Zhang and W. Xu, *Advanced Energy Materials*, 2021, **11**, 2003092.